ORIGINAL ARTICLE

Performance enhancement of a solar still using magnetic powder as an energy storage medium-exergy and environmental analysis

Ramasamy Dhivagar[1] ® | Shahin Shoeibi[2] | Hadi Kargarsharifabad[2] |
Mohammad Hossein Ahmadi[3] ® | Mohsen Sharifpur[4,5]

[1]Department of Mechanical Engineering, QIS College of Engineering and Technology, Ongole, India

[2]Energy and Sustainable Development Research Center, Semnan Branch, Islamic Azad University, Semnan, Iran

[3]Faculty of Mechanical Engineering, Shahrood University of Technology, Shahrood, Iran

[4]Department of Mechanical and Aeronautical Engineering, University of Pretoria, Pretoria, South Africa

[5]Department of Medical Research, China Medical University Hospital, China Medical University, Taichung, Taiwan

Correspondence
Ramasamy Dhivagar, Department of Mechanical Engineering, QIS College of Engineering and Technology, Ongole 523272, India.
Email: dhivagar.papers@gmail.com

Mohammad Hossein Ahmadi, Faculty of Mechanical Engineering, Shahrood University of Technology, Shahrood, Iran.
Email: mohammadhosein.ahmadi@gmail.com

Mohsen Sharifpur, Department of Mechanical and Aeronautical Engineering, University of Pretoria, Pretoria, South Africa.
Email: mohsen.sharifpur@up.ac.za

Abstract

The use of different energy storage materials can have a high effect on the water productivity of solar desalination. This study evaluates the impact of magnetic powders on modified solar still (MPSS) performance and compares the results with conventional solar still (CSS). Black iron oxide magnetic powder was selected to increase solar radiation absorption. The black iron magnetic powder simultaneously acts as a thermal storage material and a porous absorber medium. The thermal energy stored in the magnetic powder improved the performance of the MPSS during peak solar irradiation hours, resulting in higher productivity. The results showed that the thermal performance of MPSS was higher than CSS. The MPSS exhibited a 39.8% higher evaporative and 14.5% higher convective heat transfer rate compared with CSS. Results showed that the cumulative water productivity of MPSS was 31.2% greater than CSS. Also, the energy and exergy efficiencies of MPSS were improved by 18.9% and 19.04%, respectively, compared with CSS. Moreover, the predicted payback period in MPSS and CSS were 3.2 and 4.3 months. Additionally, the CO_2 reduction of MPSS was improved by approximately 45.53% compared with that of CSS. The results also showed that the exergoeconomic parameter of MPSS and CSS with energy base was equal to 33.1 and 24.56 kWh/\$, respectively.

KEYWORDS
economic, energy, exergy, magnetic iron oxide, solar still

1 | INTRODUCTION

The use of solar energy has a significant effect on human needs.[1–3] Solar energy is an unlimited source of energy, which can produce electrical power,[4–6] solar desalination,[7,8] air heating, etc. The pure water requirement is increasing dramatically in the contemporary globe compared to the previous century due to expansion in population density, industrial innovation, and agricultural requirements. According to a recent study, over 3.2 billion people live in villages to severe water shortages and water-restricted agricultural activity.[9–11] Hence, it is critical to devise a method that can meet the demand for freshwater without threatening long-term growth. Solar desalination is a method for dealing with water constraints. This technique employs the basic principles of evaporation and condensation.[12]

Numerous research have studied the factors affecting the freshwater output of solar desalination.[13] Khanmohammadi and Sabzpooshani[14] increased the water generation of weir-type cascade solar desalination by different types of nano/PCM. TiO_2, CuO, and GO nanopowders were dispersed in the PCM to keep high the water productivity at the night. Their results indicated that the highest hourly water output of the nanopowders is obtained in solar desalination using CuO/PCM, which was about $9.28 \, kg/m^2$. Arunkumar et al.[15] used paraffin wax as a PCM in hemispherical solar desalination with a concentrator. In this experiment, six copper balls (28 mm diameter) were attached to the basin and found a productivity improvement of $4.46 \, kg/m^2$. In the solar still, Naim and Abd El-Kawi[16] employed a phase change material by the mixture of paraffin wax, water, and aluminum turnings. The enhanced productivity and efficiency were about $4.53 \, kg/m^2$ and 36.2%, respectively. Patel and Kumar[17] tested the impact of HP-500 thermic fluids at a water height of 0.02 m and discovered an 11.24% rise in productivity than conventional solar still (CSS). Rufuss et al.[18] evaluated the impact of various nano/PCM on the freshwater generation of solar still. The body of solar still was connected with PCM to enhance the freshwater output of the system at low solar intensity. Their findings revealed that the water output of the system using TiO_2, CuO, and GO nanopowders in PCM was equal to 4.940, 5.280, and $3.660 \, L/m^2$.

Many studies have focused on using nanomaterials/nanofluids to boost solar still productivity.[19–22] Omara et al.[23] employed nanofluid in an active system and observed a 180% increase in productivity over CSS at 1 cm water height. Sharshir et al.[24] enhanced the freshwater generation of solar still using nanoparticles. They reported that using 1% CuO micro-flakes boosted solar still generation by 44.91%. Kabeel et al.[25] investigated the efficiency of a solar desalination system by nanofluid and external condenser. The results showed that the productivity of the solar stills using nanofluid and condenser was raised by 53.2% and 116%, respectively. Rashidi et al.[26] studied the influence of nanofluids on stepped solar desalination. The results revealed that raising the nanoparticle concentration from 0% to 5% increased hourly productivity by 22%. With the effect of copper oxide nanofluid in varied concentrations, Nazari et al.[27] increased the solar desalination performance. Over the CSS, it has increased its productivity, energy, and exergy efficiency. Parsa et al.[28] discovered that solar desalination performed better than CSS by using a nanofluid and external condenser. They discovered that the silver nanoparticles boosted the productivity while simultaneously acting as an antimicrobial.

Some of the research works were carried out in solar stills using a magnetic field to enhance the overall productivity.[29–31] Dumka et al.[32] employed ring magnets in a solar still and boosted evaporation and productivity by 49.2% and 23.5% over CSS. It boosted convective heat transfer and productivity by 48% and 38%, respectively, according to Mehdizadeh Youshanlouei et al.[33] To improve CSS productivity, energy, and exergy efficiency by 21.7%, 31.3%, and 22.6%, Dubey and Mishra[34] employed ring magnets and galvanized iron sheet metal. Sadeghi and Nazari[35] improved water output and energy efficiency by 218% and 117% over CSS by an active system with magnetic nanofluid (0.08%). Dhivagar and Mohanraj[36] used graphite plate fins and magnets to increase exergy and energy efficiencies by 1.81% and 21.46% above CSS. Dhivagar et al.[37] found that using block and disc magnets in CSS increased productivity by 31.7% and 23.7%, respectively.

The cost-effectiveness of solar desalination was assessed for economic aspects.[38,39] The various parameters of economic analysis, such as exergoeconomic, enviroeconomic, and enviroexergoeconomic analysis assists to achieve a cost-effective design of devices.[40,41] Yousef et al.[42] used numerous energy storage media in CSS and got a cost per liter (CPL) of 0.0343 $. Using altitude ideas, Parsa et al.[43] employed the economic analysis of a solar still device in the Touchal mountain. They reported that the CPL in traditional and modified systems was 0.0079 $ and 0.0372 $, respectively. Shoeibi et al.[44] employed the performance of the double slope solar desalination with nanofluid for increasing the evaporation and condensation area. Different nanoparticles, including MWCN, TiO_2, AL_2O_3, and CuO were dispersed into the water as a nanofluid. The results revealed that the CO_2 mitigation directly affects concentrations of nanopowders. In another study by

Shoeibi et al.,[45] the environmental parameters of solar desalination using thermoelectric were evaluated. The results revealed that the use of a thermoelectric module and heat sink increases the environmental parameters of the system.

The employment of different methods, including nanotechnology, phase change material, solar collector, photovoltaic/thermal panels has considerable effects on the water productivity of solar still. However, there is none of the research work reported on solar desalination using magnetic powder as a heat storage material to raise the performance of the system. In this study, the impact of magnetic powder on productivity improvement in modified solar still (MPSS) was assessed on an energy, exergy, and economic basis and compared the outcomes with CSS. Black iron oxide magnetic powder was selected to increase the adsorption of solar radiation. The black iron magnetic powder simultaneously acts as a heat storage material and a porous medium. The black iron oxide magnetic powder increases solar radiation absorption, stores thermal energy during the day, and releases it when the solar radiation is low. Also, environmental and CO_2 mitigation analysis was conducted for the view of environmental pollution reduction of solar desalination system.

2 | EXPERIMENTAL ANALYSIS

This paper evaluated the performance of CSS and modified solar. Black iron oxide magnetic powder with a weight of 0.1kg was poured into the basin of the MPSS to increase the water productivity of the system. Figure 1 indicates the MPSS and CSS schematic views. The dimensions of modified and CSSs are the same. The galvanized iron single-slope solar desalination was constructed with a basin area of 0.5 m^2 with a thickness of 0.004 m. The glass wool was used as insulation with a thickness of 0.025 m to decrease heat loss. The 0.005 m thick glass cover is 15° tilted (for Ongole, Andhra Pradesh) and closes the top. It is also kept vapor tight using a silicon sealant. Black paint was coated at the basin of the device to enhance solar radiation absorption. The water depth in both solar stills was 0.04 m at the beginning of the experiments. The freshwater is collected using a trough, which is fixed under the inclined glass cover and then poured in the measuring jar. The experimental view of MPSS is shown in Figure 2. The experiments on modified and CSS were performed in different days to increase the accuracy of the results.

The tests were obtained in Ongole (15.50°N 80.04°E), India. The trials employed a solar still facing south. The quantity of about 40 g of magnetic powder was used for 1 kg of water in the solar desalination basin and the thermal conductivity and magnetic field strength were observed at 7.7 W/mK and 24 mT, respectively. The tests were carried out during summer climatic conditions of April-2021 (from 9:00 h to 18:00 h). The measuring data such as various temperatures, solar radiation, wind velocity, and productivity were noted for every hour intervals. A continual supply of feed water flowed into the solar still to compensate for water loss from the basin. Finally, the deposited salt content was removed from the solar still basin.

3 | ASSUMPTION FOR ENERGY AND EXERGY ANALYSIS

The following assumptions were made to find the energy and exergy efficiencies of a solar still[46]:

- There are no vapor leaks.
- Kinetic, potential, and chemical impacts are not considered.
- Saline water temperature remains constant for an hour.
- Inside the system, the temperature distribution is considered to be uniform.
- Heat leaks were ignored.
- The water depth remains constant.
- The solar irradiation strikes the basin directly.

4 | THEORETICAL BACKGROUND

4.1 | Energy analysis

The energy efficiency of solar desalination is observed using the following relation[47]:

$$\eta_{E,ss} = \frac{m_w \times L}{A_{ss} \times \sum I_{ss} \times 3600}, \tag{1}$$

where m_w shows the hourly water productivity and is calculated by the following formula:

$$m_w = \frac{h_{eva,w-g}(T_w - T_g) \times 3600}{L}, \tag{2}$$

where $h_{eva w-g}$ is the evaporative heat transfer coefficient and is obtained by

$$h_{eva\ w-g} = 0.016 h_{c,w-g} \frac{(P_w - P_g)}{(T_w - T_g)}, \tag{3}$$
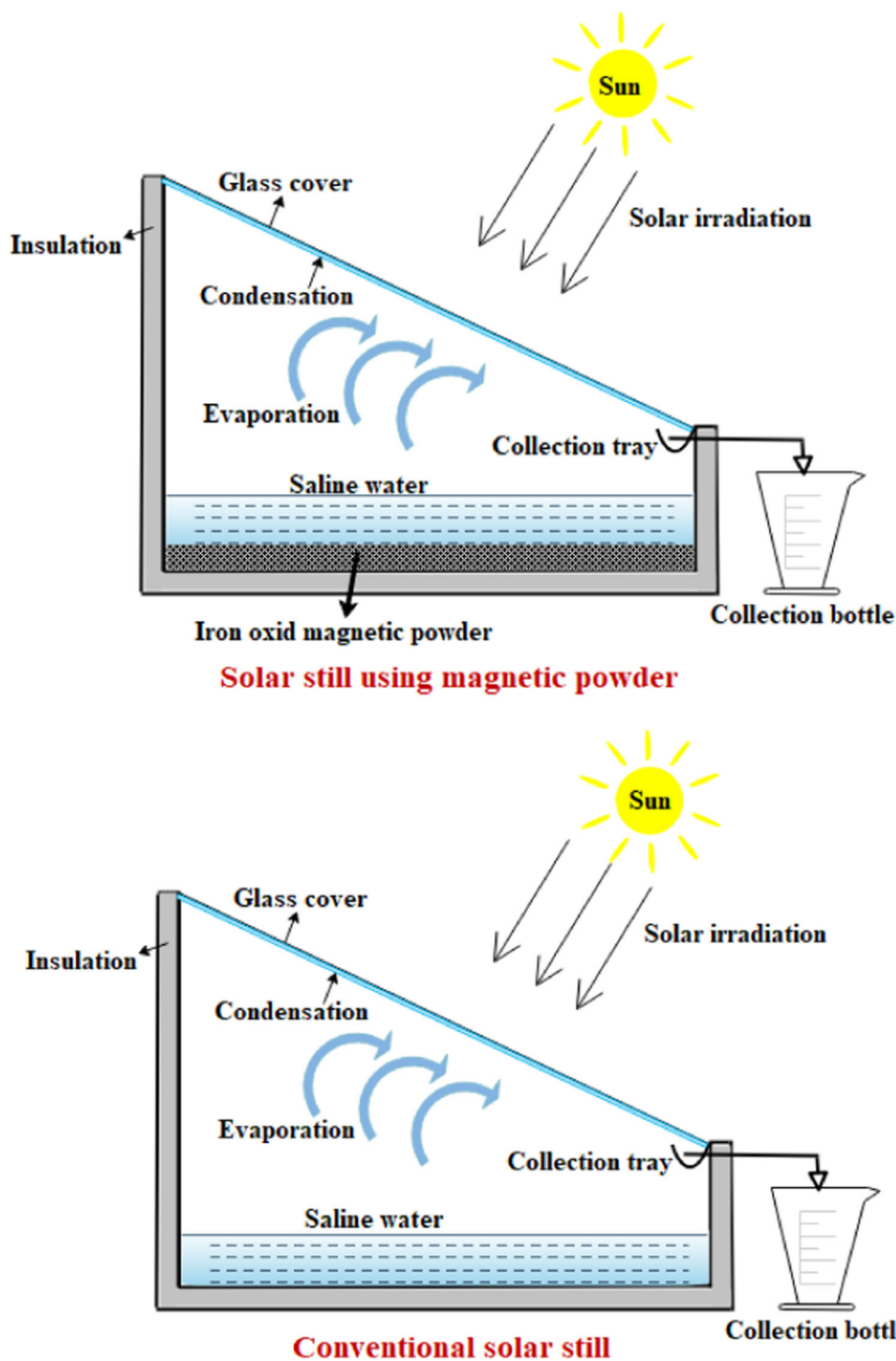
FIGURE 1 Schematic view of MPSS and CSS. CSS, conventional solar still; MPSS, modified solar still.

Where the $h_{c,w-g}$ displays the convective heat transfer coefficient between glass and water and is shown by

$$h_{c,w-g} = 0.884 \left[T_w - T_g + \frac{(P_w - P_g)T_w + 273}{268,900 - P_w} \right]^{1/3}.$$

(4)

The latent heat of vaporization is shown by

$$L = 2.4935 \times 10^6 \times [1 - 9.4779 \times 10^{-4} T_w + 1.3132 \times 10^{-7} \times T_w^2 - 4.794 \times 10^{-9} \times T_w^3]$$

(5)

for $T_w < 70°C$,

FIGURE 2 Experiment view of MPSS. MPSS, modified solar still.

TABLE 1 The uncertainty of measuring device

Equipment	Accuracy	Range	Uncertainty
Kipp-zonen solarimeter (Wm^{-2})	1	0–5000	0.6
Thermometer (°C)	0.1	−100 to 1300	0.06
Anemometer (m/s)	0.1	0-10	0.06
Volume meter (ml)	0.2	0-10	0.115

$$L = 3.1615 \times (10^6 - 761.6 T_w) \text{ for } T_w > 70^\circ C. \tag{6}$$

4.2 | Exergy analysis

The exergy performance of a device is assessed to quantify the energy losses in solar desalination.[48]

The exergy output of a solar still:

$$Ex_{out} = Ex_{eva} = \frac{\sum m_w \times L \times \left(1 - \frac{T_a + 273}{T_w + 273}\right)}{3600}. \tag{7}$$

The exergy input of a solar still:

$$Ex_{in} = Ex_s = A_{ss} \times \sum I_s \times \left[1 - \frac{4}{3} \times \left(\frac{T_a + 273}{T_s}\right) + \frac{1}{3} \times \left(\frac{T_a + 273}{T_s}\right)^4\right]. \tag{8}$$

The exergy efficiency:

$$\eta_{Ex} = \frac{\sum Ex_{eva}}{\sum Ex_s}. \tag{9}$$

4.3 | Uncertainty analysis

During the experimentation, K-type thermocouples were considered to measure all temperatures such as water, cover, ambient, and air vapor mixture with an accuracy of $\pm 0.1°C$. The solar irradiation was measured with a solarimeter with ± 1 W/m^2 precision. The van anemometer measured wind velocity to ± 0.1 m/s precision. The distillate was calculated using a calibrated flask with ± 5 ml accuracy.

The uncertainty parameter was conducted on experimental data. The standard uncertainty was calculated by following formula[49]:

$$u = \frac{a}{\sqrt{3}}, \tag{10}$$

where a displays the accuracy of the measuring device and u is the standard uncertainty. Table 1 shows the experimental instrument uncertainties.

Holman[50] estimated measurement uncertainty using the precision of each measuring device, and the appropriate equation is presented.

$$w_r = \left[\left(\frac{\partial R}{\partial x_1} w_1\right)^2 + \left(\frac{\partial R}{\partial x_2} w_2\right)^2 + \cdots + \left(\frac{\partial R}{\partial x_n} w_n\right)^2\right]^{1/2}. \tag{11}$$

R denotes the function, w_r denotes the entire uncertainty, x denotes the independent variable, and w is the independent variable with regard to the uncertainty. Replacing the daily thermal efficiency into Equation (11) gives the uncertainty of the thermal efficiency by

$$u(\eta_{E,ss}) = \left[\left(\frac{L}{A_{ss} \times \sum I_{ss} \times 3600}\right)^2 \cdot u^2(m_w)\right.$$
$$\left. + \left(\frac{1}{(A_{ss} \times \sum I_{ss} \times 3600)^2}\right)^2 \cdot u^2(I_{ss})\right]^{0.5} \tag{12}$$

In addition, by replacing the exergy efficiency into Equation (11), the uncertainty of exergy efficiency is obtained by

$$u(\eta_{Ex}) = \left[\left(\frac{1}{Ex_s}\right)^2 \cdot u^2(Ex_{eva}) + \left(\frac{Ex_{eva}}{Ex_s^2}\right)^2 \cdot u^2(Ex_s)\right]^{0.5}. \tag{13}$$

By computing the above equations, the highest uncertainties related to energy efficiency and exergy efficiency in solar desalination are 1.42% and 2.1%, respectively.

5 | ECONOMIC AND ENVIRONMENTAL ANALYSIS

5.1 | Cost per liter

The economic viability of a solar still is estimated at the price of 1 L of distilled water.[51] The fixed annual cost (FAC) of the device is obtained by[52]

$$FAC = CRF \times CC, \tag{14}$$

where CC is the construction cost of the device. The capital recovery factor (CRF) is assumed by

$$CRF = \frac{i(1+i)^n}{(1+i)^n - 1}. \tag{15}$$

Here, i is the interest rate of 12%, and n is 10 years lifetime of solar desalination. The annual salvage value (ASV) is shown by

$$ASV = SSF \times S. \tag{16}$$

The salvage value (S) is estimated by

$$S = 0.2 \times CC. \tag{17}$$

The sinking fund factor (SFF) is assumed by

$$SFF = \frac{i}{(1+i)^n - 1}. \tag{18}$$

The annual maintenance cost (AMC) of the system:

$$AMC = 0.15 \times FAC. \tag{19}$$

The annual cost (AC) is estimated using the following relation:

$$AC = FAC + AMC - ASV. \tag{20}$$

The CPL of distillate is found by

$$CPL = \frac{AC}{P_d}. \tag{21}$$

Here, P_d represents the average annual freshwater generation during 270 days.[53] The payback period (PBP) of the system is estimated by

$$PBP = \frac{Investments}{Net\ earnings}. \tag{22}$$

5.2 | Exergoeconomic analysis

The exergoeconomic parameter was considered to optimize the economic design of solar desalination with considering the exergy analysis and is shown by[42]

$$R_{Ex} = \frac{(E_{ex})_{out}}{AC} \tag{23}$$

$$R_{En} = \frac{(E_{en})_{out}}{AC}, \tag{24}$$

where R_{Ex} and R_{En} present the exergoeconomic parameter based on exergy and energy.

5.3 | CO₂ removal

The annual net amount of CO_2 reduction in the device is achieved by $E_{product} \times n \times 2$ and is calculated by[54]

$$\varphi_{co_2,en} = \frac{2((E_{en})_{out} \times n)}{1000}, \tag{25}$$

$$\varphi_{co_2,ex} = \frac{2((E_{ex})_{out} \times n)}{1000}. \tag{26}$$

5.4 | Enviroeconomic parameter

The enviroeconomic parameter is extracted as the price obtained by the CO_2 reduction during the lifespan of the device and is shown by[45]

$$Z_{co_2} = z_{co_2} \times \varphi_{co_2}. \tag{27}$$

The value of CO_2 is about 14.5\$ per ton.[47]

5.5 | Profit cost ratio (PCR)

The BCR is a technique for the cost evaluation of the device and is calculated by[55]

$$PCR = \frac{UAB}{AC}, \qquad (28)$$

where UAB represents the present cost of the benefit. The present cost of benefit in the device is calculated by following formula[56]:

$$UAB = M \times POW, \qquad (29)$$

where POW displays the price of freshwater (supposed 0.10 \$/L). The profit price ratio must be more than unity so that the investment is efficient.

6 | RESULTS AND DISCUSSIONS

In the Ongole climatic conditions during the month of April 2021, the experimentation results were observed for the performance comparison.

6.1 | Variations of ambient parameters

Figure 3 illustrates the variations in solar irradiations and wind velocity. It is noted that the solar radiation was increasing from morning 11:00 h to afternoon 14:00 h during the experimentations. Afterward, it was reduced in the evening from 16:00 to 18:00 h. During this time length, the maximum solar irradiation was observed to be 932.4 W/m² at 14:00 h and the minimum value was obtained at 18:00 h as 34.2 W/m², respectively. In these hours, the formation of clouds also plays a vital role in affecting the intensity of solar irradiation, reducing the system efficiency. Regarding wind velocity, the values were ranging from 1.3 to 2.5 m/s during the experimentation. The flow of wind over the surface of the experiment setup was unpredictable during the observation hours. The curve formation denoted in Figure 2 is also not in the predicted way. During the experimentation, the maximum and minimum observed wind velocity was 1.26 and 2.47 m/s, respectively. Wind velocity's impact on the glass cover's surface accelerates the condensation process, which gives higher productivity.[57]

Figure 4 depicts the variations in different temperatures. During the experimentation, the observed maximum ambient temperature was 39.2°C at 14:00 h. It was reduced gradually as solar irradiation reduces during evening hours. Afternoon high glass cover temperature
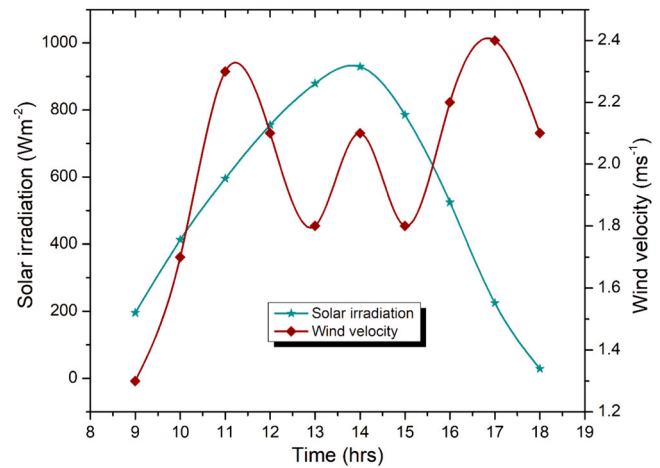

FIGURE 3 Solar irradiation and wind velocity during the test

of 50.2°C was recorded (14:00 h). The glass cover temperature affects the internal water and air-vapor mixture temperature. The uneven flow of wind also can be the reason for influencing this glass cover temperature. It dropped over the day, as expected. The MPSS's highest air-vapor temperature was 61.3°C, requiring the use of magnetic material in the basin layer. In MPSS, the noted air-vapor temperature was 13.3% higher than CSS. It is understood that the heat accumulation at the surface of saline water significantly improved the air-vapor temperature in MPSS, resulting in a higher evaporation rate. The saline water temperature in MPSS reached the highest value of about 59.2°C during 14:00 h, resulted in higher water output. As a result of the heat energy contained in magnetic powder, the MPSS saline water temperature was 11.9% higher than CSS. This has increased evaporation and productivity in MPSS.

The convective and evaporative heat transfer variations in MPSS and CSS are depicted in Figure 5. The convective heat transfer increased gradually from morning to afternoon, peaking at 1.65 W/m²K in MPSS and 1.41 W/m²K in CSS. The noted enhancement in MPSS was 14.5% higher than CSS due to the surface heat of saline water improvement by magnetic powder. The observed evaporate heat transfer in MPSS and CSS was about 26.8 W/m²K and 16.3 W/m²K, respectively at 14:00 h. This enhancement in MPSS was 39.8% higher than CSS. Because of the lower density of water vapor due to the magnetic field, quicker evaporation and convection heat transfer occur during increased solar irradiation hours.

6.2 | Variations of productivity

The quantity of obtained productivity was changed from morning to evening hours throughout the day. The hourly
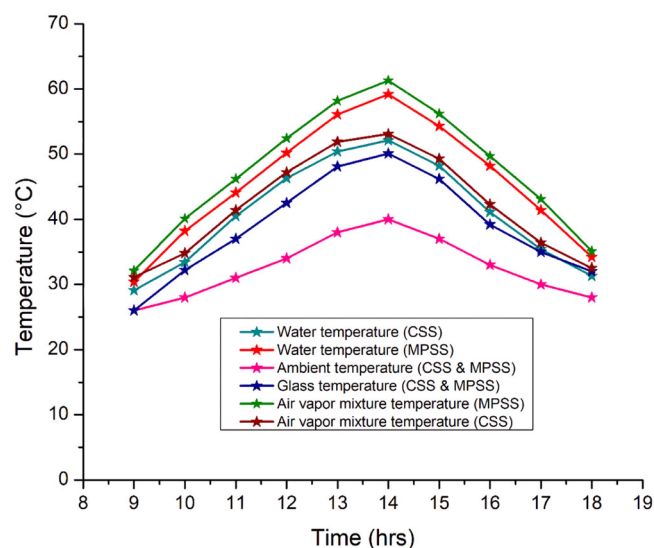
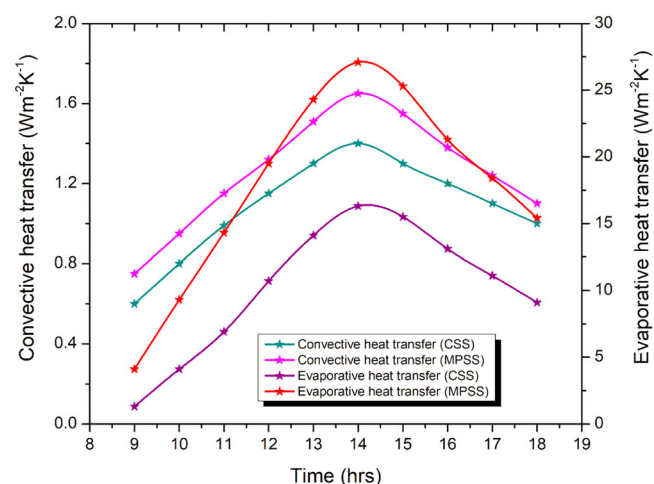**FIGURE 4** Variations of different temperatures during experimentation

FIGURE 5 Variations of different temperatures during experimentation

FIGURE 6 Hourly and accumulative productivities of the device.

productivity was maximum during afternoon hours and decreased when solar irradiation was reduced. Figure 6 illustrates variations in hourly and cumulative productivity. It is proportional to solar irradiation. The maximum hourly productivity was enhanced during peak solar irradiation in both the solar stills. In MPSS, the maximum hourly productivity was improved to about 580 ml at 14:00 h and in CSS, it was about 470 ml only. The observed hourly productivity in MPSS is 18.9% higher than CSS due to the heat storage effect and magnetization observed using magnetic powder. This also happens due to the raise in water temperature in MPSS. In this way, the magnetic powder absorbs maximum solar irradiation in the basin region, increasing water temperature. The higher heat
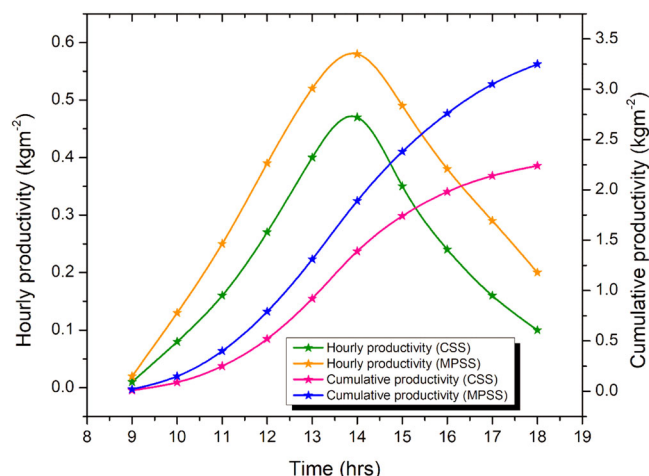
buildup for water vaporization in MPSS occurs due to enhanced heat transfer between saline water and cover. The study found that MPSS with magnetic powder outperforms CSS. Both solar stills reached their peak combined productivity at 14:00 h. These were 3.26 kg/m² for MPSS and 2.24 kg/m² for CSS. The collected productivity in MPSS was 31.2% higher than in CSS.

6.3 | Energy and exergy efficiencies

The variations of energy and exergy efficiencies are depicted in Figure 7. The impact of magnetic field exhibited in MPSS energy efficiency compared to CSS. At 14:00 h, MPSS reached its peak energy efficiency of around 28.5%. Afterward, it was reduced as solar energy was reduced. The highest energy efficiency in CSS was about 23.1% which is 18.9% lower than MPSS. The stored energy influenced by the magnetic field significantly enhanced the energy efficiency in MPSS than CSS. Furthermore, it is denoted that using magnetic powder has increased the exergy efficiency in MPSS when compared to CSS. The hourly exergy efficiency for both solar desalination was increased from the start of the experiment to 14.00 h. In MPSS, it was about 4.2% which is 19.04% more than CSS. The maximum exergy efficiency in CSS was 3.4%. In general, for all solar stills, the exergy efficiency is poor.

6.4 | Economic and environmental viability

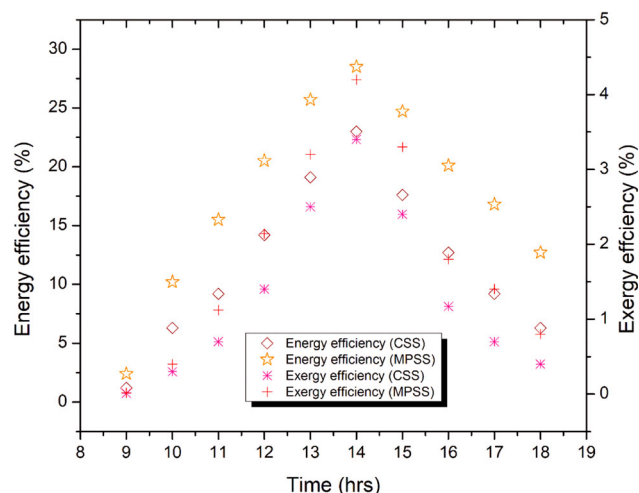The economic analysis was used to assess the cost-effectiveness of MPSS and CSS, which is illustrated in

FIGURE 7 Variations of energy and exergy efficiencies

TABLE 2 CPL analysis of CSS and MPSS

Parameters	CSS	MPSS
CC	81.79 $	88.49 $
CRF	0.177	0.177
FAC	14.47 $	15.66 $
S	16.35	17.69
SFF	0.056	0.056
ASV	0.91	0.99
AMC	2.17 $	2.34 $
AC	15.73 $	17.04 $
P_d	604.8 kg	880.2 kg
CPL	0.026 $	0.019 $
PBP	4.3 months	3.2 months

Abbreviations: CPL, cost per liter; CSS, conventional solar still; MPSS, modified solar still.

Table 2. The basin and glass cover are cleaned regularly to prevent corrosion. These charges were considered in the capital cost estimate. The CPL of productivity in MPSS was evaluated at 0.019 $, which is 26.9% lower than CSS. Furthermore, the estimated PBP for MPSS and CSS was about 3.2 and 4.3 months, respectively. The increase in solar irradiation and productivity reduces the CPL and PBP considerably.[57]

Table 3 presents the exergoeconomic parameter in the lifespan of 10 years and interest rates of 12%. As observed, the exergoeconomic parameter in the MPSS with exergy and energy base was higher than CSS, due to high freshwater production of the solar desalination with magnetic powders as an energy storage media. As observed, the exergoeconomic parameter of MPSS and CSS with energy base was equal to 33.1 and 24.56 kWh/$, respectively.

Table 4 shows the CO_2 reduction and enviroeconomic parameters of solar desalination for a lifespan of 10 years. As observed, the CO_2 reduction of MPSS was improved by approximately 45.53% compared to CSS, due to highe freshwater output of the solar desalination with magnetic powders. The outcomes showed that the enviroeconomic parameter of MPSS and CSS was about 163.1 $ and 386.4 $, respectively.

TABLE 4 Environmental and enviroeconomic parameters of MPSS and CSS

Parameter	MPSS	CSS
Life time (years)	10	10
Annual energy generation (kWh)	526.3	386.4
Annual exergy generation (kWh)	32.78	22.52
CO_2 removal during lifespan (tons)	11.25	7.73
Enviroeconomic parameter ($)	163.1	112.1

Abbreviations: CSS, conventional solar still; MPSS, modified solar still.

TABLE 3 Exergoeconomic parameter for MPSS and CSS

Type	n (year)	i (%)	Annual $(E_{en})_{out}$ (kWh)	nnual $(E_{ex})_{out}$ (kWh)	AC ($)	R_{En} (kWh/$)	R_{Ex} (kWh/$)
MPSS							
	10	12	562.3	37.78	17.04	33.1	1.92
CSS							
	10	12	386.4	22.52	15.73	24.56	1.43

Abbreviations: CSS, conventional solar still; MPSS, modified solar still.

TABLE 5 Profit cost ratio of CSS and MPSS

Type of solar still	*n* (year)	i (%)	AC ($)	POW ($)	*M* (L/year)	UAB ($)	PCR
CSS	10	12	15.73	0.10	604.8	60.4	3.83
MPSS	10	12	17.04	0.10	880.2	88.4	5.19

Abbreviations: CSS, conventional solar still; MPSS, modified solar still.

TABLE 6 The water output and economic analysis of different system

Type of system	References	Annual freshwater yield (L/m^2)	CPL ($/L)
Pyramid solar still	[58]	1510	0.021
Tubular using Parabolic concentrator	[59]	92	0.29
Stepped solar still using vacuum tube solar collector	[60]	1360	0.039
Solar still using thermoelectric cooling and solar collector	[61]	438	0.13
CSS	This study	604	0.026
MPSS	This study	880	0.019

Abbreviations: CPL, cost per liter; CSS, conventional solar still; MPSS, modified solar still.

Table 5 displays the profit cost ratio of CSS and MPSS. The results revealed that conventional and modified solar PCR still is more than unity. It can be seen that the profit price ratio of MPSS was about 35.4% higher than traditional ones.

Table 6 displays the CPL and water output in different configurations of solar desalination. The results indicated that the CPL for MPSS using magnetic powder was lower than the other solar stills. Also, the highest annual freshwater yield was obtained in pyramid solar still, which was about 1510 L/m^2.

7 | CONCLUSION

The use of different media as an energy storage material is a technical method to obtain high water generation in solar still. The present paper evaluated the performance of the solar desalination device with magnetic powders as an energy storage material. This modification leads to an enhanced evaporation rate of saline water and increased water productivity. Also, the energy, exergy, economic, exergoeconomic, and environmental parameters of both MPSS and CSS devices were compared. The MPSS and CSS were tested in the identical climatic circumstances, and the following conclusions were reached:

- The water temperature of the MPSS system was improved by 11.9% higher than CSS.

- The evaporation and convection rates of the MPSS system were increased by 39.8% and 14.5%, respectively, compared with CSS.
- The black magnetic powder significantly impacts water productivity and CPL of MPSS.
- The use of magnetic powder in the water of MPSS raised the cumulative productivity by 31.2% higher than CSS.
- The CO_2 reduction of MPSS was improved approximately 45.53% compared to CSS.
- The maximum energy and exergy efficiencies observed in MPSS were 18.9% and 19.04% higher than in CSS, respectively.
- The enviroeconomic parameter of MPSS and CSS was about 163.1 $ and 386.4 $, respectively.
- The CPL of MPSS and CSS found was found to be 0.026 and 0.019 $/L, respectively.
- The PBP for MPSS is approximately 3.2 months compared to 4.3 months for a CSS.
- The exergoeconomic parameter of MPSS and CSS with energy base was equal to 33.1 and 24.56 kWh/$, respectively.

NOMENCLATURE

A	surface area (m^2)
AC	annual cost ($)
AMC	annual maintenance cost ($)
ASV	annual salvage value ($)
CRF	capital recovery factor

CC	Construction cost ($)
CSS	conventional solar still
E	energy (W)
E_x	exergy (W)
FAC	first annual cost ($)
h	heat transfer co-efficient (W/m²K)
$I(t)$	incident solar energy (W/m²)
K	thermal conductivity (W/mK)
L	latent heat of evaporation (kJ/kg)
m	hourly distillate (kg)
MPSS	magnetic powder solar still
P	pressure (N/m²)
PBP	payback period (months)
PCR	profit cost ratio
POW	price of fresh water
R	exergoeconomic (kWh/$)
UAB	present cost of profit
T	temperature(K)

GREEK SYMBOL

| η | efficiency (%) |
| φ_{CO_2} | CO₂ mitigation (tons) |

SUBSCRIPTS

a	ambient air
c	convection
eva	evaporation
g	glass
in	input energy
out	output energy
s	sun
w	water

ORCID

Ramasamy Dhivagar https://orcid.org/0000-0002-2775-7930

Mohammad Hossein Ahmadi https://orcid.org/0000-0002-0097-2534

REFERENCES

1. Selmy AE, Soliman M, Allam NK. Refractory plasmonics boost the performance of thin-film solar cells. *Emerg Mater.* 2018;1(3):185-191.
2. Malinkiewicz O, Imaizumi M, Sapkota SB, Ohshima T, Öz S. Radiation effects on the performance of flexible perovskite solar cells for space applications. *Emerg Mater.* 2020;3(1):9-14.
3. Pegu M, Haris MPU, Kazim S, Ahmad S. Understanding and harnessing the potential of layered perovskite-based absorbers for solar cells. *Emerg Mater.* 2020;3(6):751-778.
4. Sultan SM, Tso CP, Efzan E. A case study on effect of inclination angle on performance of photovoltaic solar

thermal collector in forced fluid mode (in English). *Renew Energy Res Appl.* 2020;1(2):187-196.
5. Guada M, Moretón A, Rodríguez-Conde S, et al. Daylight luminescence system for silicon solar panels based on a bias switching method. *Energy Sci Eng.* 2020;8(11):3839-3853.
6. Ghahremani A, Fathy AE. A three-dimensional multiphysics modeling of thin-film amorphous silicon solar cells. *Energy Sci Eng.* 2015;3(6):520-534.
7. Goshayeshi HR, Chaer I, Yebiyo M, Öztop HF. Experimental investigation on semicircular, triangular and rectangular shaped absorber of solar still with nano-based PCM. *J Therm Anal Calorim.* 2022;147(4):3427-3439.
8. Adibi Toosi SS, Goshayeshi HR, Zeinali Heris S. Experimental investigation of stepped solar still with phase change material and external condenser. *J Energy Storage.* 2021;40:102681.
9. Amin ZM, Hawlader MNA. Analysis of solar desalination system using heat pump. *Renew Energy.* 2015;74:116-123.
10. Dhivagar R, Mohanraj M. Optimization of performance of coarse aggregate-assisted single-slope solar still via Taguchi approach (in English). *J Renew Energy Environ.* 2021;8(1):13-19.
11. Dhivagar R, Mohanraj M, Belyayev Y. Performance analysis of crushed gravel sand heat storage and biomass evaporator-assisted single slope solar still (in English). *Environ Sci Pollut Res Int.* 2021;28(46):65610-65620.
12. Goshayeshi HR, Safaei MR. Effect of absorber plate surface shape and glass cover inclination angle on the performance of a passive solar still. *Int J Numer Methods Heat Fluid Flow.* 2020;30(6):3183-3198.
13. Safaei MR, Goshayeshi HR, Chaer I. Solar still efficiency enhancement by using graphene oxide/paraffin nano-PCM. *Energies.* 2019;12(10):2002.
14. Khanmohammadi S, Sabzpooshani M. Theoretical assessment of a solar still system equipped with nano-phase change materials. *Int J Green Energy.* 2020;18(2):111-127.
15. Arunkumar T, Denkenberger D, Ahsan A, Jayaprakash R. The augmentation of distillate yield by using concentrator coupled solar still with phase change material. *Desalination.* 2013;314:189-192.
16. Naim MM, Abd El Kawi MA. Non-conventional solar stills part 1. Non-conventional solar stills with charcoal particles as absorber medium. *Desalination.* 2003;153(1):55-64.
17. Patel P, Kumar R. Comparative performance evaluation of modified passive solar still using sensible heat storage material and increased frontal height. *Proc Technol.* 2016;23:431-438.
18. Dsilva Winfred Rufuss D, Suganthi L, Iniyan S, Davies PA. Effects of nanoparticle-enhanced phase change material (NPCM) on solar still productivity. *J Clean Prod.* 2018;192:9-29.
19. Asbik M, Boushaba H, Hafs H, Koukouch A, Sabri A, Muthu Manokar A. Investigating the effect of sensible and latent heat storage materials on the performance of a single basin solar still during winter days. *J Energy Storage.* 2021;44:103480.
20. Prasad AR, Attia MEH, Al-Kouz W, Afzal A, Athikesavan MM, Sathyamurthy R. Energy and exergy efficiency analysis of solar still incorporated with copper plate and phosphate pellets as energy storage material (in English). *Environ Sci Pollut Res Int.* 2021;28(35):48628-48636.

21. Benoudina B, Attia MEH, Driss Z, Afzal A, Manokar AM, Sathyamurthy R. Enhancing the solar still output using micro/nano-particles of aluminum oxide at different concentrations: an experimental study, energy, exergy and economic analysis. *Sustain Mater Technol.* 2021;29:e00291.

22. Dhindsa GS, Kumar V, Mittal MK, et al. Performance comparison of single-slope solar still loaded with various nanofluids. *Energy Sci Eng.* 2021:1-14

23. Omara ZM, Kabeel AE, Essa FA. Effect of using nanofluids and providing vacuum on the yield of corrugated wick solar still. *Energy Convers Manage.* 2015;103:965-972.

24. Sharshir SW, Peng G, Wu L, et al. Enhancing the solar still performance using nanofluids and glass cover cooling: experimental study. *Appl Therm Eng.* 2017;113:684-693.

25. Kabeel AE, Omara ZM, Essa FA. Numerical investigation of modified solar still using nanofluids and external condenser. *J Taiwan Inst Chem Eng.* 2017;75:77-86.

26. Rashidi S, Bovand M, Rahbar N, Esfahani JA. Steps optimization and productivity enhancement in a nanofluid cascade solar still. *Renew Energy.* 2018;118:536-545.

27. Nazari S, Safarzadeh H, Bahiraei M. Performance improvement of a single slope solar still by employing thermoelectric cooling channel and copper oxide nanofluid: an experimental study. *J Clean Prod.* 2019;208:1041-1052.

28. Parsa SM, Rahbar A, Koleini MH, Aberoumand S, Afrand M, Amidpour M. A renewable energy-driven thermoelectric-utilized solar still with external condenser loaded by silver/nanofluid for simultaneously water disinfection and desalination. *Desalination.* 2020;480:114354.

29. Dhivagar R. A concise review on productivity and economic analysis of Auxiliary-component-assisted solar stills. *Energy Technol.* 2021;9(11):2100501.

30. Dhivagar R, Kannan KG. Thermodynamic and economic analysis of heat pump-assisted solar still using paraffin wax as phase change material (in Eng). *Environ Sci Pollut Res Int.* 2022;29(2):3131-3140.

31. Dsilva Winfred D, Arulvel S, Anil Kumar V, et al. Combined effects of composite thermal energy storage and magnetic field to enhance productivity in solar desalination. *Renew Energy.* 2022;181:219-234.

32. Dumka P, Kushwah Y, Sharma A, Mishra DR. Comparative analysis and experimental evaluation of single slope solar still augmented with permanent magnets and conventional solar still. *Desalination.* 2019;459:34-45.

33. Mehdizadeh Youshanlouei M, Yekani Motlagh S, Soltanipour H. The effect of magnetic field on the performance improvement of a conventional solar still: a numerical study (in English). *Environ Sci Pollut Res Int.* 2021;28(24):31778-31791.

34. Dubey M, Mishra DR. Thermo-exergo-economic analysis of double slope solar still augmented with ferrite ring magnets and GI sheet. *Desalin Water Treat.* 2020;198:19-30.

35. Sadeghi G, Nazari S. Retrofitting a thermoelectric-based solar still integrated with an evacuated tube collector utilizing an antibacterial-magnetic hybrid nanofluid. *Desalination.* 2021;500:114871.

36. Dhivagar R, Mohanraj M. Performance improvements of single slope solar still using graphite plate fins and magnets. *Environ Sci Pollut Res.* 2021;28(16):20499-20516.

37. Dhivagar R, Mohanraj M, Deepanraj B, Murugan VS. Assessment of single slope solar still using block and disc magnets via productivity, economic, and enviro-economic perspectives: a comparative study (in English) *Environ Sci Pollut Res Int.* 2021:1-9abe0-79c9-4d09-a876-65a3cbc943d2">1-9.

38. Dhivagar R, Sundararaj S. Thermodynamic and water analysis on augmentation of a solar still with copper tube heat exchanger in coarse aggregate. *J Therm Anal Calorim.* 2018;136(1):89-99.

39. Jeevadason AW, Padmini S, Bharatiraja C, Kabeel AE. A review on diverse combinations and Energy-Exergy-Economics (3E) of hybrid solar still desalination. *Desalination.* 2022;527:115587.

40. Amirrud MR, Shahin M. Sensitivity and uncertainty analysis of economic feasibility of establishing wind power plant in kerman, Iran (in English). *Renew Energy Res Appl.* 2020;1(2):247-260.

41. Abdelgaied M, Attia MEH, Kabeel AE, Zayed ME. Improving the thermo-economic performance of hemispherical solar distiller using copper oxide nanofluids and phase change materials: experimental and theoretical investigation. *Sol Energy Mater Sol Cells.* 2022;238:111596.

42. Yousef MS, Hassan H, Sekiguchi H. Energy, exergy, economic and enviroeconomic (4E) analyses of solar distillation system using different absorbing materials. *Appl Therm Eng.* 2019;150:30-41.

43. Parsa SM, Rahbar A, Javadi Y D, Koleini MH, Afrand M, Amidpour M. Energy-matrices, exergy, economic, environmental, exergoeconomic, enviroeconomic, and heat transfer (6E/HT) analysis of two passive/active solar still water desalination nearly 4000m: altitude concept. *J Clean Prod.* 2020; 261:121243.

44. Shoeibi S, Rahbar N, Abedini Esfahlani A, Kargarsharifabad H. Improving the thermoelectric solar still performance by using nanofluids– experimental study, thermodynamic modeling and energy matrices analysis. *Sustain Energy Technol Assess.* 2021;47:101339.

45. Shoeibi S. Numerical analysis of optimizing a heat sink and nanofluid concentration used in a thermoelectric solar still: an economic and environmental study. *Environ Res Eng Manag.* 2021;77(2):110-122.

46. Elango C, Gunasekaran N, Sampathkumar K. Thermal models of solar still—a comprehensive review. *Renew Sustain Energy Rev.* 2015;47:856-911.

47. Shoeibi S, Kargarsharifabad H, Rahbar N, Ahmadi G, Safaei MR. Performance evaluation of a solar still using hybrid nanofluid glass cooling-CFD simulation and environmental analysis. *Sustain Energy Technol Assess.* 2022;49:101728.

48. Shoeibi S, Kargarsharifabad H, Rahbar N, Khosravi G, Sharifpur M. An integrated solar desalination with evacuated tube heat pipe solar collector and new wind ventilator external condenser. *Sustain Energy Technol Assess.* 2022;50:101857.

49. Hassani M, Rahbar N. Application of thermoelectric cooler as a power generator in waste heat recovery from a PEM fuel cell–an experimental study. *Int J Hydrogen Energy.* 11/16 2015;40:15040-15051.

50. Holman JP. *Experimental Methods for Engineers.* McGraw-Hill; 2001.

51. Shoeibi S, Rahbar N, Esfahlani AA, Kargarsharifabad H. Energy matrices, exergoeconomic and enviroeconomic analysis of air-cooled and water-cooled solar still: experimental investigation and numerical simulation. *Renew Energy*. 2021;171:227-244.

52. Shoeibi S, Kargarsharifabad H, Mirjalily SAA, Zargarazad M. Performance analysis of finned photovoltaic/thermal solar air dryer with using a compound parabolic concentrator. *Appl Energy*. 2021;304:117778.

53. Dhivagar R, Mohanraj M, Hidouri K, Belyayev Y. Energy, exergy, economic and enviro-economic (4E) analysis of gravel coarse aggregate sensible heat storage-assisted single-slope solar still. *J Therm Anal Calorim*. 2021;145(2):47.

54. Shoeibi S, Kargarsharifabad H, Mirjalily SAA, Muhammad T. Solar district heating with solar desalination using energy storage material for domestic hot water and drinking water—environmental and economic analysis. *Sustain Energy Technol Assess*. 2022;49:101713.

55. Kosmadakis G, Manolakos D, Kyritsis S, Papadakis G. Economic assessment of a two-stage solar organic ankine cycle for reverse osmosis desalination. *Renew Energy*. 2009;34(6):1579-1586.

56. Singh AK, Poonia S, Jain D, Mishra D. Performance evaluation and economic analysis of solar desalination device made of building materials for hot arid climate of India. *Desalin Water Treat*. 2019;141:36-41.

57. Mohanraj M, Karthick L, Dhivagar R. Performance and economic analysis of a heat pump water heater assisted regenerative solar still using latent heat storage. *Appl Therm Eng*. 2021;196:117263.

58. Fath HES, El-Samanoudy M, Fahmy K, Hassabou A. Thermal-economic analysis and comparison between pyramid-shaped and single-slope solar still configurations. *Desalination*. 2003;159(1):69-79.

59. Elashmawy M, Alshammari F. Atmospheric water harvesting from low humid regions using tubular solar still powered by a parabolic concentrator system. *J Clean Prod*. 2020;256:120329.

60. Kabeel AE, Khalil A, Omara ZM, Younes MM. Theoretical and experimental parametric study of modified stepped solar still. *Desalination*. 2012;289:12-20.

61. Esfahani JA, Rahbar N, Lavvaf M. Utilization of thermo-electric cooling in a portable active solar still—an experimental study on winter days. *Desalination*. 2011;269(1-3):198-205.

APPENDIX

The values observed in solving energy balance equations are as follows:

$$P_g = \exp\left[25.317 - \frac{5144}{T_g + 273}\right], \tag{A1}$$

$$P_w = \exp\left[25.317 - \frac{5144}{T_w + 273}\right]. \tag{A2}$$